

---

# BEYOND PERCEPTUAL DISTANCES: RETHINKING DISPARITY ASSESSMENT FOR OUT-OF-DISTRIBUTION DETECTION WITH DIFFUSION MODELS

---

Kun Fang<sup>1</sup>, Qinghua Tao<sup>2</sup>, Zuopeng Yang<sup>3</sup>, Xiaolin Huang<sup>1</sup> and Jie Yang<sup>1</sup>

<sup>1</sup>Department of Automation, Shanghai Jiao Tong University, {fanghenshao, xiaolinhuang, jieyang}@sjtu.edu.cn

<sup>2</sup>ESAT-STADIUS, KU Leuven, Belgium, qinghua.tao@esat.kuleuven.be

<sup>3</sup>Guangzhou University, yzpeng44@gmail.com

## ABSTRACT

Out-of-Distribution (OoD) detection aims to justify whether a given sample is from the training distribution of the classifier-under-protection, i.e., In-Distribution (InD), or from OoD. Diffusion Models (DMs) are recently utilized in OoD detection by using the perceptual distances between the given image and its DM generation. DM-based methods bring fresh insights to the field, yet remain under-explored.

In this work, we point out two main limitations in DM-based OoD detection methods: (i) the perceptual metrics on the disparities between the given sample and its generation are devised only at human-perceived levels, ignoring the abstract or high-level patterns that help better reflect the intrinsic disparities in distribution; (ii) only the raw image contents are taken to measure the disparities, while other representations, i.e., the features and probabilities from the classifier-under-protection, are easy to access at hand but are ignored. To this end, our proposed detection framework goes beyond the perceptual distances and looks into the deep representations from the classifier-under-protection with our novel metrics devised correspondingly, leading to more informative disparity assessments between InD and OoD. An anomaly-removal strategy is integrated to remove the abnormal OoD information in the generation, further enhancing the distinctiveness of disparities. Our work has demonstrated state-of-the-art detection performances among DM-based methods in extensive experiments.

## 1 Introduction

Deep Neural Networks (DNNs) have shown superior generalization ability on the In-Distribution (InD) data, i.e., the training dataset [1]. However, DNNs give unreliable predictions when encountering new data from an out distribution  $\mathbb{P}_{\text{out}}$  that differs from the InD  $\mathbb{P}_{\text{in}}$ , which can pose fetal safety issues under open-world environments [2]. A large number of researches have been conducted on detecting the Out-of-Distribution (OoD) data, which is the well-known OoD detection problem [3].

Recently, Diffusion Models (DMs) [4] have been utilized in OoD detection [5, 6, 7]. The key idea lies in that DMs can generate high-fidelity images from the learned distribution. In these methods, a DM pre-trained on the InD data is adopted to generate images  $\hat{x}$  that align well with InD. Then, the *disparities* between the given input sample  $x$  and its DM-generated  $\hat{x}$  help distinguish whether  $x$  is from InD or OoD, since the disparities can be more pronounced for OoD inputs compared to those InD inputs. Thus, DM-based methods introduce new perspectives to the field of OoD detection by looking into the generative images.

Currently, DM-based detection methods remain less studied, compared to other DNN-based methods [8, 9, 10, 11, 12], whereas the generation process and the involved disparity information are promising to be better utilized. The existing DM-based works focus on the techniques for the enhanced generation of  $\hat{x}$  and then calculate the perceptual disparities between the given input image  $x$  and its DM generation  $\hat{x}$  [5, 6, 7]. The pioneering work [5] firstly leverages the forward and reverse diffusion processes on the input image  $x$  to generate a synthesis  $\hat{x}$ . The named DiffGuard [7] follows up by

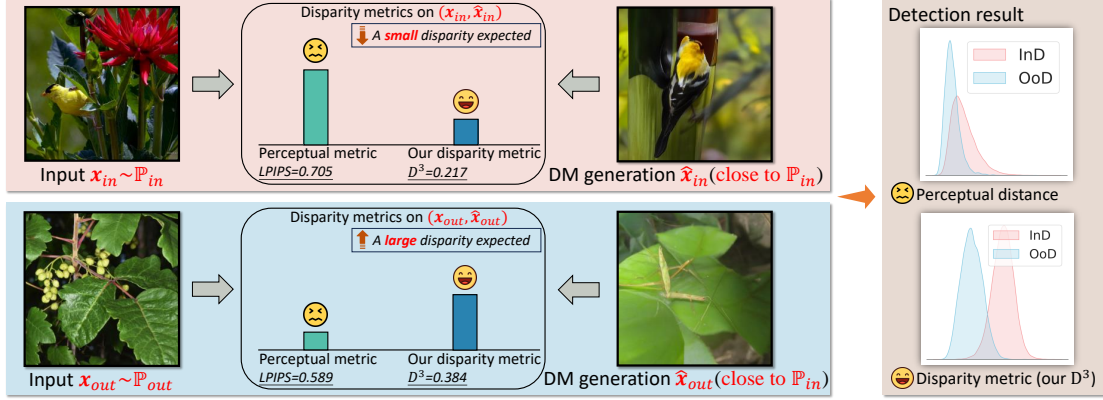


Figure 1: Motivation for informative disparity assessments. (i) Given an InD image  $x_{in}$ , its DM generation  $\hat{x}_{in}$  has a small disparity in distribution with  $x_{in}$ . However, due to the rich and unique image contents, a large perceptual distance is obtained between  $x_{in}$  and  $\hat{x}_{in}$ , e.g.,  $LPIPS(x_{in}, \hat{x}_{in})$ . (ii) Given a OoD image  $x_{out}$ , its DM generation  $\hat{x}_{out}$  should have a large distribution disparity with  $x_{out}$ . However, due to the resembling local image structure and texture, a small perceptual distance, e.g.,  $LPIPS(x_{out}, \hat{x}_{out})$ , is obtained, leading to unsatisfactory results.  $D^3$  leverages deep representations with our devised metrics, enhancing the separability in assessing InD and OoD.

improving the reverse diffusion process of generating  $\hat{x}$  for more distinctive semantic mismatches between  $x$  and  $\hat{x}$ , attaining state-of-the-art (SOTA) detection performance. In [6], it proposes to corrupt  $x$  to lift it off its distribution, and then generates  $\hat{x}$  by inpainting the corrupted  $x$  through the pre-trained DM model.

With DMs, we note two key aspects that play crucial roles in yielding good OoD detection performances, i.e., (i) *the objectives taken in assessments* and (ii) *the metrics used in disparity measurements*. However, the existing DM-based methods have limitations in both of these aspects.

- **The assessed objectives:** The raw image contents are simply taken as the objective for the assessment procedures [5, 6, 7]. Besides those human-perceived image contents, there are other levels of representations that could be more related to the data distribution, such as the network responses of features and probabilities from the classifier-under-protection. Such information is in practice easy to access at hand under the OoD detection setups, but is currently ignored in the existing work.
- **The measured metrics:** The perceptual metrics directly used on the image contents are calculated to describe the disparities, e.g., the LPIPS distance [13] in [5, 6] and the DISTS distance [14] in [7]. Such measurements remain at human-perceived levels, e.g., the texture and structure, and may even mislead the intrinsic disparities in the distributions between  $x$  and its generation  $\hat{x}$ , as exemplified in Fig.1. Hence, more authentic metrics can be considered for better reflecting the InD and OoD disparities, especially when it comes to comparing other objectives, such as the aforementioned network responses of the image.

In this work, we propose a new DM-based framework for OoD detection through rethinking the existing two limitations above. In our proposed method, it goes beyond the raw image contents as the comparing objectives, but exerts diverse and more informative representations from the network of the classifier-under-protection. Correspondingly, novel metrics are devised for enhanced disparity measurements under diverse comparing objectives. The novelty and contributions of our work are summarized as follows.

- *We leverage the representations in the feature and probability spaces of the classifier-under-protection as the objectives to assess.* Rather than the image contents at human-perceived levels, more abstract and informative representations can be learned from the classifier-under-protection which is trained on the InD data, facilitating to pronounce the disparities between InD and OoD.
- *Two disparity metrics are devised for the representations from the leveraged feature space and probability space.* The  $\ell_2$ -distance has been justified to capture feature disparities between InD and OoD [10, 11] and is integrated into our devised metric for feature representations; the Kullback-Leilber (KL) divergence is incorporated into our devised metric for probability representations.

- An anomaly-removal strategy is further integrated into our framework by removing the abnormal responses from the DM-generated synthesis  $\hat{x}$ . In this way, the distribution disparities between  $x$  and  $\hat{x}$  can get enhanced in both two spaces, thereby facilitating a more accurate assessment of the proposed metrics.

## 2 Related work

### 2.1 Out-of-distribution detection

Given a sample  $x \in \mathbb{R}^d$  in the inference stage of the classifier-under-protection, the OoD detection task is formulated as a bi-classification problem with a decision function  $D(\cdot)$  and a scoring function  $S(\cdot)$ :

$$D(x) = \begin{cases} \text{InD}, & S(x) > s, \\ \text{OoD}, & S(x) < s. \end{cases} \quad (1)$$

If the detection score  $S(x)$  is greater than a threshold  $s$ , the decision function  $D(x)$  views  $x$  as an InD sample, vice versa. The threshold  $s$  is determined such that most of the InD samples can be correctly classified. The key to successful OoD detection lies in an authentic scoring function  $S(\cdot)$  that well describes the disparities between InD and OoD.

Typical non-DM based detection methods leverage distinct responses w.r.t. the input image  $x$  from the classifier-under-protection, i.e., the logits [8, 15, 16, 17, 9], the parameter gradients [12, 18], and the network features [19, 10, 20, 21, 22, 11]. Proper metrics are then used on such responses to quantify the likelihood of  $x$  being from the InD, such as the energy function on logits [9], the distances [19, 10, 20] and reconstruction errors [22, 11] on features, or the gradient norms [12].

### 2.2 Diffusion models

Diffusion Models (DMs), or saying diffusion denoising probabilistic models, have achieved great successes in generating high-fidelity images from the learned distribution [4, 23]. In DMs, the so-called *forward* and *reverse* diffusion processes are involved, where a generated image can be obtained for any given input image.

- Forward process: An image  $x$  is corrupted with  $T$  steps of Gaussian noises until it turns into pure noises  $x_T$ :

$$q(x_t|x_{t-1}) = \mathcal{N}(x_t|\sqrt{1-\beta_t}x_{t-1}, \beta_t\mathbf{I}), \quad (2)$$

where  $0 \leq t \leq T$  and  $\beta_t$  follows a fixed variance schedule so that  $x_T$  is close to an isotropic Gaussian  $\mathcal{N}(\mathbf{0}, \mathbf{I})$ .

- Reverse process: A neural network with parameters  $\theta$  is introduced to remove the noises in  $x_T$  via multiple steps, until a clean image  $\hat{x} = p_\theta(x_0|x_T)$  is finally recovered:

$$p_\theta(x_{t-1}|x_t) = \mathcal{N}(x_{t-1}|\mu_\theta(x_t, t), \Sigma_\theta(x_t, t)), \quad (3)$$

where  $\mu_\theta$  and  $\Sigma_\theta$  are learned mean and variances of Gaussian noises from the neural network with  $\theta$ .

### 2.3 OoD Detection with diffusion models

DMs have recently been applied to OoD detection, where the generation ability makes it promising and different from classical supervised DNNs widely used in OoD detection [9, 12, 11]. Given a DM pre-trained on InD data, a test image from an unknown distribution is firstly corrupted via adding noises and then gets denoised, following the forward and reverse diffusion processes. It is widely agreed that the resulting image  $\hat{x}$  is generated *close to* the InD  $\mathbb{P}_{\text{in}}$ , since the DM is pre-trained on InD data for its generative capability. Therefore, an OoD input image  $x_{\text{out}} \in \mathbb{P}_{\text{out}}$  in general has more distinctive dissimilarities with its generation  $\hat{x}_{\text{out}}$  from the DM, while an InD input  $x_{\text{in}} \in \mathbb{P}_{\text{in}}$  exhibits less discrepancies with  $\hat{x}_{\text{in}}$ . Such discrepancy in distribution between  $x$  and  $\hat{x}$  can be utilized for OoD detection. Hence, the existing DM-based methods [5, 6, 7] focus on the disparities between the image and its DM-generated synthesis for OoD detection, which is also the main focus of our investigations. We note that in [24] a DM is used to generate photo-realistic OoD images as data augmentation for additionally training a bi-classifier, but this falls outside the unsupervised setups and the primary focus of this work.

In [5], the pioneering DM-based OoD detection method is proposed by corrupting the given image  $x$  at a range of different noise levels and generating the recovered images  $\hat{x}$ . Then [6] proposes to mask  $x$  in order to lift it off its distribution, and employs DMs to inpaint the masked image. A recent work [7] develops multiple test-time techniques in the reverse process of DMs to generate images  $\hat{x}$  with larger semantic differences from original images  $x$ . Those existing

methods all adopt perceptual metrics, i.e., LPIPS [13] and DISTS [14], on the given image  $x$  and its DM-generated  $\hat{x}$  as the scoring function to decide the detection results. However, the adopted perceptual metrics reflect the distances on human-perceived patterns in the raw image contents, such as the textures, which do not necessarily capture the intrinsic distribution disparities of images, as shown with the counter examples in Fig.1.

### 3 D<sup>3</sup>: Diffusion Distribution Disparity

In this work, we argue that two key aspects need to be well addressed in DM-based OoD detectors: (i) the objectives for assessments and (ii) the metrics for measurements. Correspondingly, a novel DM-based detection framework is proposed, as shown in Fig.2 that integrates the informative representations in the feature and probability spaces from the classifier-under-protection and devises corresponding metrics to jointly measure the distribution disparities between  $x$  and  $\hat{x}$ . The proposed detection framework is named as **Diffusion Distribution Disparity (D<sup>3</sup>)**, involving the effective metrics in Sec.3.1 for features and probabilities and also an anomaly-removal strategy in Sec.3.2.

**Notations.** Given an image  $x \in \mathbb{R}^d$  to detect, its DM-generated synthesis is denoted as  $\hat{x} \in \mathbb{R}^d$ . The classifier-under-protection  $f : \mathbb{R}^d \rightarrow \mathbb{R}^C$  learns penultimate-layer features  $h_x, h_{\hat{x}} \in \mathbb{R}^m$  of the images  $x, \hat{x}$ , and gives the probabilities  $g_x, g_{\hat{x}} \in \mathbb{R}^C$  in the classification layer. Here,  $h_x, h_{\hat{x}}$  imply the feature representations of  $x, \hat{x}$  from the network of the classifier-under-protection, while  $g_x, g_{\hat{x}}$  imply the classification probability representations by applying a softmax function on the logits of  $x, \hat{x}$ .

#### 3.1 Novel assessments on feature and probability representations of images

The raw image contents, e.g., the texture and structure at the human-perceived level, can be insufficient to measure the disparity in distribution between  $x$  and  $\hat{x}$ , as shown in Fig.1. Hence, our work advocates to utilize more informative representations regarding the images. Under the OoD detection setups, the network of classifier-under-protection is trained on the InD data and is available at hand. Thus, besides the generative information from DMs, the classifier-under-protection also contains useful information about the InD, which is yet not utilized in the assessment of existing DM-based detection methods [5, 6, 7].

In our work, we investigate both representations in the feature space and probability space from the classifier-under-protection for measuring the distribution disparities in  $x$  and  $\hat{x}$ . Generally, the distribution disparities in OoD detection tasks contain two types: the covariate shift and the concept shift [25]. The former usually refers to the changes in image styles, e.g., photography v.s. cartoon. Such changes do not alter the category, and can be reflected in the feature space. The latter refers to the changes in semantic labels, e.g., cats v.s. dogs, and thus can be identified in the probability space.

**D<sup>3</sup> on features.** The classifier network being protected is trained on InD data, enabling it to learn informative features for InD inputs. However, when given with OoD inputs, it can attain features that lack meaningful representations. In this regard, the covariate shift in features can be evident in the fact that InD features are more concentrated and comparatively distant from OoD features [10]. Therefore, we leverage the  $\ell_2$  distance on the obtained features to effectively capture the disparities between InD and OoD.

Given features  $h_x, h_{\hat{x}}$  of  $x, \hat{x}$ , we adopt the  $\ell_2$  distance on the normalized features  $h_x, h_{\hat{x}}$  from the classifier-under-protection to assess the disparity in  $x, \hat{x}$ :

$$\epsilon_{\ell_2}(x, \hat{x}) = \epsilon_{\ell_2}(h_x, h_{\hat{x}}) = \left\| \frac{h_{\hat{x}}}{\|h_{\hat{x}}\|_2} - \frac{h_x}{\|h_x\|_2} \right\|_2. \quad (4)$$

In our metric in Eq.(4), the  $\ell_2$ -normalization  $\|\cdot\|_2$  is also applied to  $h_x, h_{\hat{x}}$ , which normalizes the feature norms for more distinctive characteristics on InD data as elucidated in [10, 11]. Hence, a small  $\ell_2$  distance between  $h_x$  and  $h_{\hat{x}}$  implies that  $x$  is more likely to come from InD, while a large  $\ell_2$  distance suggests  $x$  being more possible as an OoD sample, because the DM is trained on InD data and its generation  $\hat{x}$  appears more close to InD as explained in Sec.2.3.

**D<sup>3</sup> on probabilities.** Aside from the  $\ell_2$ -distance based metric on features in Eq.(4), we further consider the concept shift on probabilities regarding the classification labels through the celebrated Kullback-Leibler (KL) divergence, which quantifies the distribution distance between a given probability distribution  $p$  and a reference one  $q$ :  $D_{\text{KL}}(p \parallel q) = \sum_i p_i \log(p_i/q_i)$  [26]. Given the probabilities  $g_x, g_{\hat{x}}$  of  $x, \hat{x}$  from the classifier-under-protection, the following metric  $\epsilon_{\text{KL}}$  captures the concept shift in an input  $x$  with the help of its DM generation  $\hat{x}$  and a uniform probability  $u = [1/C, \dots, 1/C] \in \mathbb{R}^C$  on the  $C$  classes:

$$\epsilon_{\text{KL}}(x, \hat{x}) = \epsilon_{\text{KL}}(g_x, g_{\hat{x}}) = \frac{D_{\text{KL}}(g_{\hat{x}} \parallel u)}{D_{\text{KL}}(g_x \parallel u)}. \quad (5)$$

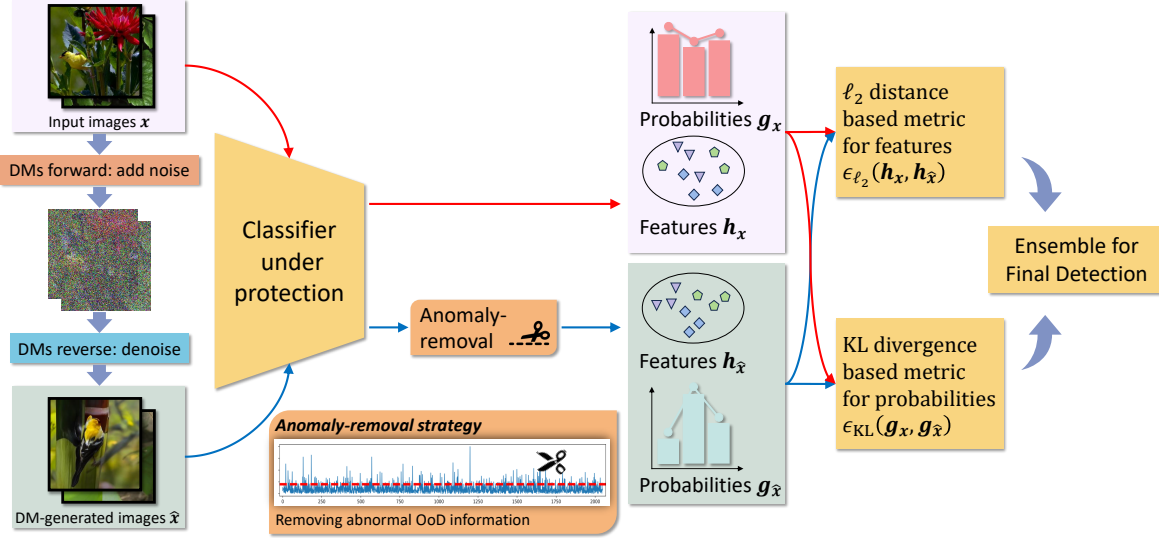


Figure 2: Schematic illustration of  $D^3$ . The classifier-under-protection is introduced to calculate the distribution disparity between a test image  $x$  and its DM generation  $\hat{x}$  in the learned feature space and probability space. An anomaly-removal strategy removes the abnormal OoD information hidden in the DM-generated  $\hat{x}$  for more significant distribution disparities and enhanced detection performance.

We would like to highlight the importance of the uniform probability  $u$  in Eq.(5) from two aspects: (i) what a uniform  $u$  indicates and (ii) why  $u$  is necessary in our  $\epsilon_{KL}$ .

- As discussed in [12], an InD sample tends to produce a probability with a peak value in its ground-truth class, while an OoD sample leans towards being assigned a uniform probability, e.g.,  $u$ , as the classification category of OoD is beyond those of InD. In this sense, the uniform probability  $u$  serves as a good approximation for the classifying probabilities of OoD data.
- In the definition of KL-divergence, i.e.,  $D_{KL}(p \parallel q) = \sum_i p_i \log(p_i/q_i)$ ,  $p$  indicates the observed data distribution while  $q$  represents a theoretical approximation of  $p$ , and thus  $D_{KL}$  is interpreted as the discrepant information through using  $q$  to model  $p$ . As both  $g_x$  and  $g_{\hat{x}}$  indicate the *observations* regarding InD and OoD, it is essential to introduce the uniform  $u$  as the reference  $q$  to *approximate* the OoD in  $D_{KL}$ .

**Ensemble on features and probabilities.** The metric  $\epsilon_{\ell_2}$  on features and  $\epsilon_{KL}$  on probabilities provide distinct perspectives on capturing the distribution disparities between  $x$  and  $\hat{x}$ , together contributing to the two types of shifts in OoD data. To fully leverage the representations in such two spaces, the ensemble of  $\epsilon_{\ell_2}$  and  $\epsilon_{KL}$  is taken as the scoring function of  $D^3$  for comprehensive disparity assessments with a balancing coefficient  $\lambda \in [0, 1]$ :

$$S(x) = \lambda/\epsilon_{KL}(x, \hat{x}) + (1 - \lambda)/\epsilon_{\ell_2}(x, \hat{x}). \quad (6)$$

### 3.2 An anomaly-removal strategy

In  $D^3$ , the DM pre-trained on InD data learns to capture informative patterns from the InD  $\mathbb{P}_{in}$ . Thus, given any test image  $x$ , the generated  $\hat{x}$  is consistently learned to align with  $\mathbb{P}_{in}$ , regardless of whether  $x$  is from  $\mathbb{P}_{in}$  or  $\mathbb{P}_{out}$ . An anomaly-removal strategy is designed in  $D^3$  to boost the distribution disparity by forcing  $\hat{x}$  more aligned with  $\mathbb{P}_{in}$ .

Generally in the network of classifier-under-protection, the extremely high or low values in the penultimate-layer features  $h_x$  commonly contain abnormal information and can be truncated, which have been exploited in non-DM-based OoD detection methods [27, 28, 29, 30]. In our proposed  $D^3$  framework, we justify that such abnormal information also exists in the generated images  $\hat{x}$  from DMs. Correspondingly, we conduct feature pruning to remove the anomaly information residing in the features  $h_{\hat{x}}$  of the classifier-under-protection  $f(\cdot)$  w.r.t. the DM-generated images  $\hat{x}$ , as illustrated in Fig.2.

To be specific, we truncate the learned features  $\mathbf{h}_{\hat{x}}$  via the acknowledged ReAct [27] and VRA [30] techniques due to their cheap computation costs, such that

$$\mathbf{h}_{\hat{x}}^{\text{RA}} = \min(\mathbf{h}_{\hat{x}}, c), \mathbf{h}_{\hat{x}}^{\text{VRA}} = \begin{cases} 0, & \mathbf{h}_{\hat{x}} < \alpha, \\ \mathbf{h}_{\hat{x}}, & \alpha \leq \mathbf{h}_{\hat{x}} \leq \beta, \\ \beta, & \mathbf{h}_{\hat{x}} > \beta, \end{cases} \quad (7)$$

where  $c$  and  $\alpha, \beta (\alpha < \beta)$  are the chosen constants. We then attain the rectified features  $\mathbf{h}_{\hat{x}}^{\text{RA}}, \mathbf{h}_{\hat{x}}^{\text{VRA}}$  from the penultimate layer, which correspondingly yield the rectified probabilities  $\mathbf{g}_{\hat{x}}^{\text{RA}}, \mathbf{g}_{\hat{x}}^{\text{VRA}}$  of  $\hat{x}$  in the classification layer. In this way, anomaly information in  $\hat{x}$  can be removed, so that the representations of  $\hat{x}$  in the two spaces are more aligned with InD  $\mathbb{P}_{\text{in}}$  and exhibit more distinctive disparities with that of  $\mathbf{x}$ . To differentiate the pruning techniques, we denote our methods as  $D^3$  and  $D^{3+}$  w.r.t. the ReAct [27] and VRA [30] techniques, respectively, leading to the final scoring functions of  $D^3$  and  $D^{3+}$  with Eq.(6) as follows:

$$\begin{aligned} S_{D^3}(\mathbf{x}) &= \lambda/\epsilon_{\text{KL}}(\mathbf{g}_{\mathbf{x}}, \mathbf{g}_{\hat{x}}^{\text{RA}}) + (1 - \lambda)/\epsilon_{\ell_2}(\mathbf{h}_{\mathbf{x}}, \mathbf{h}_{\hat{x}}^{\text{RA}}), \\ S_{D^{3+}}(\mathbf{x}) &= \lambda/\epsilon_{\text{KL}}(\mathbf{g}_{\mathbf{x}}, \mathbf{g}_{\hat{x}}^{\text{VRA}}) + (1 - \lambda)/\epsilon_{\ell_2}(\mathbf{h}_{\mathbf{x}}, \mathbf{h}_{\hat{x}}^{\text{VRA}}). \end{aligned} \quad (8)$$

Note that the focus of our anomaly-removal strategy differs from those feature-pruning methods w.r.t. the detection framework and decision scores [27, 30], despite the shared goal of wiping OoD information. Firstly, the latter is non-DM based and tackles the the input image  $\mathbf{x}$ , while ours is operated on the DM-generated reference image  $\hat{x}$ . Secondly, regarding the detection score, the latter further relies on an additional logits-based score, e.g., Energy [9], on the altered logits, while ours directly compares the outputs of  $\mathbf{x}$  and its DM generation  $\hat{x}$  to attain detection scores following our devised metric in Eq.(8).

## 4 Experiments

In this section, experiments are conducted extensively to evaluate the proposed  $D^3$  with comparisons to varied existing methods based on generic DNNs and DMs. Implementation details of  $D^3$  can be find in Appendix A.3. Our source code will be released.

### 4.1 Setups

**Benchmarks.** Our experiments are based on a prevalent OpenOOD [31] benchmark, which provides a variety of InD and OoD datasets, detectors, checkpoints, etc. In experiments, we consider the large-scale ImageNet-1K dataset [32] with an image size of  $224 \times 224 \times 3$  as the InD. The CIFAR10 dataset [33] with a very small size of  $32 \times 32 \times 3$  is omitted, as the powerful generation ability of diffusion models can only be fully exerted on high-resolution images. For the OoD data, following the settings in [7], 4 datasets are selected from the OpenOOD: Species [34], iNaturalist [35], OpenImage-O [36] and ImageNet-O [37], with details provided in Appendix A.1.

Two metrics are calculated to evaluate the detection performance: False Positive Rate (FPR) of OoD samples at a 95% true positive rate on InD samples, and Area Under the Receiver Operating Characteristic Curve (AUROC), as widely adopted in the OpenOOD benchmark [31].

**Baselines.** Two types of methods are considered as baselines in comparisons:

- *Non-diffusion-based:* MSP [8], ODIN [15], Energy [9], GradNorm [12], ViM [36], KNN [10], MLS [16], ReAct [27] and VRA [30]. These detection methods cover the logits-/features-/gradients-based types, and are widely recognized as effective detection methods.
- *Diffusion-based:* A pioneering work DDPM [5] detection method and a recent superior one DiffGuard [7].

All these strong baselines are post-hoc and can be conveniently executed on standard DNNs in inference, without requirements of re-training or structure modifications. More details are given in Appendix A.2.

**Diffusion models.** The checkpoints released by OpenAI<sup>1</sup> are adopted [38] and are trained on the training set of ImageNet-1K. In the main comparisons of Sec.4.2, we use the conditional  $256 \times 256$  diffusion model, and adopt the DDIM sampling [39] to accelerate the generation speed. More varied settings on the diffusion model are analyzed in Sec.4.4, including unconditional diffusion models and varied sampling time steps. We do not consider another popular

<sup>1</sup><https://github.com/openai/guided-diffusion>

method	OoD data sets								AVERAGE	
	Species		iNaturalist		OpenImage-O		ImageNet-O			
	FPR↓	AUROC↑	FPR↓	AUROC↑	FPR↓	AUROC↑	FPR↓	AUROC↑	FPR↓	AUROC↑
<i>non-diffusion-based</i>										
MSP [8]	79.52	75.16	52.71	88.42	63.58	84.98	100.00	28.64	73.95	69.30
ODIN [15]	80.89	72.88	50.87	91.14	57.29	89.23	100.00	40.87	72.26	73.53
Energy [9]	82.33	72.04	53.83	90.61	57.10	89.15	100.00	41.91	73.31	73.43
GradNorm [12]	74.42	75.70	26.95	93.87	47.67	85.07	95.60	48.16	61.16	75.70
ReAct [27]	68.65	77.39	19.69	96.37	43.93	90.39	98.00	52.39	57.57	79.13
KNN [10]	76.19	76.38	68.41	85.12	57.56	86.45	84.65	75.37	71.70	80.83
ViM [36]	83.94	70.68	67.85	88.40	57.56	89.63	85.30	70.88	73.66	79.90
MLS [16]	80.87	72.89	50.80	91.15	57.11	89.26	100.00	40.85	72.20	73.54
VRA [30]	69.64	76.94	15.74	97.12	<u>36.42</u>	<b>92.93</b>	95.55	60.79	54.34	81.94
<i>diffusion-based</i>										
DDPM [5]	96.86	44.97	96.27	48.70	94.41	49.35	91.55	51.73	94.77	48.69
DiffGuard [7]	83.68	73.19	71.23	85.81	74.80	82.32	87.74	65.23	79.36	76.64
DiffGuard+KNN	71.04	77.81	48.79	90.19	52.80	87.80	<u>80.85</u>	<b>75.68</b>	63.37	82.87
DiffGuard+ViM	72.26	74.48	39.09	92.50	45.02	91.11	82.30	72.42	59.67	82.63
DiffGuard+MLS	70.31	75.95	30.74	93.03	40.61	90.74	87.05	65.72	57.18	81.36
D <sup>3</sup>	<b>64.81</b>	<b>81.27</b>	<b>10.65</b>	<b>97.89</b>	<b>35.58</b>	<u>92.16</u>	88.05	69.51	<b>49.77</b>	<u>85.20</u>
D <sup>3</sup> +	<u>66.45</u>	<u>81.23</u>	<u>14.67</u>	<u>97.13</u>	41.93	<u>88.70</u>	<b>80.25</b>	<u>75.51</u>	<u>50.82</u>	<b>85.64</b>

Table 1: The detection performance of a variety of OoD detectors (**ResNet50** on **ImageNet-1K**). The **best** and runner-up results are highlighted with bold fonts and underlines, respectively.

Latent Diffusion Models (LDMs) [40], as the auto-encoder encoding the latent space of LDMs is trained on a much larger data set than the ImageNet-1K. Hence, the InD of LDMs cover far more data than ImageNet-1K, which comes into conflict with the setups of OoD detection.

**Classifier-under-protection.** We employ the checkpoints of ResNet50 [41] and DenseNet121 [42] pre-trained on ImageNet-1K from PyTorch [43].

## 4.2 Main results

Table 1 shows the detection FPR and AUROC results of a variety of non-diffusion-based and diffusion-based methods. The diffusion-based DDPM [5] and DiffGuard [7] with perceptual metrics manifest much weaker performance than those non-diffusion-based ones. Specifically, DDPM adopts an average of MSE and LPIPS as the detection score, and is reported to be effective only on specific InD and OoD datasets with significant disparities in the original paper, e.g., the human face data set CelebA [44] and the digit data set SVHN [45]. On more complex image sets in Tab.1, DDPM yet shows an obvious failure in detecting OoD data from InD data. The DiffGuard with the DISTs distance shows substantial improvements over DDPM for its semantic mismatch-guided techniques in the reverse process of DMs. Still, DiffGuard needs to be combined with other non-diffusion methods to achieve competitive results.

In contrast, our proposed D<sup>3</sup>/D<sup>3</sup>+ pays attention to the distribution disparity of the deep representations in the feature space and probability space between the given test image and its generation, which leads to SOTA detection results with the lowest FPR and highest AUROC values averaged over all the evaluated OoD datasets. Our empirical findings reveal that the devised distribution disparity metric and the utilized deep representations can effectively exploit more informative discrepancies between InD and OoD, thus outperforming a broad class of both non-diffusion-based and diffusion-based methods with perceptual distances.

## 4.3 Ablation studies

**The metrics  $\epsilon_{KL}$  and  $\epsilon_{\ell_2}$ .** In this part, two sets of evaluations are conducted. Firstly, we investigate the individual effectiveness of our devised metrics  $\epsilon_{KL}$ ,  $\epsilon_{\ell_2}$  and their ensemble. Secondly, more choices aside from  $\epsilon_{KL}$ ,  $\epsilon_{\ell_2}$  are further exploited. In the probability space, we consider another alternative  $\epsilon_{KL-ALT} = D_{KL}(g_{\hat{x}}||g_x)$  that directly measures

Method	Score	OoD data sets								AVERAGE	
		Species		iNaturalist		OpenImage-O		ImageNet-O			
		FPR↓	AUROC↑	FPR↓	AUROC↑	FPR↓	AUROC↑	FPR↓	AUROC↑	FPR↓	AUROC↑
D <sup>3</sup>	$\epsilon_{\text{KL}}$	85.62	68.52	61.60	88.92	60.05	88.49	100.00	46.10	76.82	73.01
	$\epsilon_{\ell_2}$	76.45	74.86	29.96	92.95	60.44	77.14	79.65	74.16	61.62	79.78
	Ensemble	<b>64.81</b>	<b>81.27</b>	<b>10.65</b>	<b>97.89</b>	<b>35.58</b>	<b>92.16</b>	88.05	69.51	<b>49.77</b>	<b>85.20</b>
	$\epsilon_{\text{KL-ALT}}$	97.57	49.50	96.93	54.19	98.43	39.70	86.60	66.13	94.88	52.38
	$\epsilon_{\text{cos}}$	76.45	74.86	29.96	92.95	60.44	77.14	79.65	74.16	61.62	79.78
D <sup>3+</sup>	Ensemble	84.97	65.09	49.63	85.34	83.52	63.21	<b>78.40</b>	<b>75.32</b>	74.13	72.24
	$\epsilon_{\text{KL}}$	87.35	68.28	70.11	86.48	64.58	86.82	99.95	50.94	80.50	73.13
	$\epsilon_{\ell_2}$	76.45	74.86	29.96	92.95	60.44	77.14	79.65	74.16	61.62	79.78
	Ensemble	<b>66.45</b>	<b>81.23</b>	<b>14.67</b>	<b>97.13</b>	<b>41.93</b>	<b>88.70</b>	80.25	75.51	<b>50.82</b>	<b>85.64</b>
	$\epsilon_{\text{KL-ALT}}$	96.81	51.80	95.09	59.96	97.88	43.78	86.00	67.08	93.95	55.66
D <sup>3+</sup>	$\epsilon_{\text{cos}}$	76.45	74.86	29.96	92.95	60.44	77.14	79.65	74.16	61.62	79.78
	Ensemble	82.15	67.69	42.25	88.51	78.43	68.15	<b>77.50</b>	<b>76.40</b>	70.08	75.19

Table 2: The individual effects of different alternatives of the KL divergence ( $\epsilon_{\text{KL}}$  and  $\epsilon_{\text{KL-ALT}}$ ) in the probability space and the  $\ell_2$ -distance and cosine similarity ( $\epsilon_{\ell_2}$  and  $\epsilon_{\text{cos}}$ ) in the feature space.

Method	Setup	OoD data sets								AVERAGE	
		Species		iNaturalist		OpenImage-O		ImageNet-O			
		FPR↓	AUROC↑	FPR↓	AUROC↑	FPR↓	AUROC↑	FPR↓	AUROC↑	FPR↓	AUROC↑
D <sup>3</sup>	w/o removal	77.74	72.76	47.73	88.65	57.68	85.59	94.20	61.29	69.34	77.07
	Removal on $x, \hat{x}$	83.07	70.72	74.18	77.32	81.58	70.01	89.95	64.34	82.19	70.60
	Removal on $x$ only	83.48	73.74	77.24	78.57	85.51	66.19	91.45	56.86	84.42	68.84
	Removal on $\hat{x}$ only	<b>64.81</b>	<b>81.27</b>	<b>10.65</b>	<b>97.89</b>	<b>35.58</b>	<b>92.16</b>	<b>88.05</b>	<b>69.51</b>	<b>49.77</b>	<b>85.20</b>
D <sup>3+</sup>	w/o removal	77.74	72.76	47.73	88.65	57.68	85.59	94.20	61.29	69.34	77.07
	Removal on $x, \hat{x}$	74.34	78.33	36.08	92.71	59.31	81.97	81.00	72.52	62.68	81.38
	Removal on $x$ only	83.11	74.06	74.52	80.73	83.42	68.28	91.20	56.94	83.06	70.00
	Removal on $\hat{x}$ only	<b>66.45</b>	<b>81.23</b>	<b>14.67</b>	<b>97.13</b>	<b>41.93</b>	<b>88.70</b>	<b>80.25</b>	<b>75.51</b>	<b>50.82</b>	<b>85.64</b>

Table 3: Ablation studies on the anomaly-removal strategy of D<sup>3</sup>/D<sup>3+</sup> with results on each OoD dataset.

disparities in  $g_x, g_{\hat{x}}$  without a reference term  $u$ . In the feature space, we investigate a commonly used cosine similarity distance  $\epsilon_{\text{cos}} = \frac{h_{\hat{x}}^\top h_x}{\|h_{\hat{x}}\|_2 \|h_x\|_2}$ .

Table 2 shows the individual effects of our devised metrics and their alternatives. The results are attained as:

- In the probability space, the alternative  $\epsilon_{\text{KL-ALT}}$  falls inferior from our  $\epsilon_{\text{KL}}$ . This can be due to the fact that the probabilities  $g_x$  and  $g_{\hat{x}}$  are both observed data distributions and thereby cannot be used to directly model each other in the KL divergence.
- In the feature space, both the  $\ell_2$  distance and the cosine similarity  $\epsilon_{\text{cos}}$  manifest the same detection values under D<sup>3</sup> and D<sup>3+</sup>. Hence,  $\epsilon_{\text{cos}}$  can also be considered as an effective choice for the disparity metric on features. The reasons behind can be that the differences of feature clipping and feature similarity metrics do not change the order of the detection scores of samples in InD and OoD datasets, which brings the same FPR and AUROC results.
- In both sets of comparisons with  $(\epsilon_{\text{KL}}, \epsilon_{\ell_2})$  and  $(\epsilon_{\text{KL-ALT}}, \epsilon_{\text{cos}})$ , it shows that the individual metric in either feature space or probability space give distinctively inferior detection performances than their ensemble. Such results verify the significance of fully leveraging both features and probabilities from the classifier-under-protection regarding the covariate shift and concept shift [25].

**Anomaly-removal strategy on the generated image  $\hat{x}$ .** The importance of our anomaly-removal strategy on the generated  $\hat{x}$  in the forward procedure of the classifier-under-protection is highlighted in Tab.3. Aside from ours (“removal on  $\hat{x}$ ”), three alternative setups of the anomaly-removal strategy are exploited in the ablations, including D<sup>3</sup> without the removal strategy (“w/o removal”), D<sup>3</sup> with anomaly in  $x$  removed (“removal on  $x$ ”) and D<sup>3</sup> with anomaly in  $x$  and  $\hat{x}$  both removed (“removal on  $x, \hat{x}$ ”).



As shown in Tab.3, among all the four cases, only our devised anomaly-removal strategy on  $\hat{x}$  (“removal on  $\hat{x}$ ”) leads to good detection performances. By removing the abnormal information in the DM generation  $\hat{x}$ , we enhance its alignment with InD, thereby rendering the disparities between  $x$  and  $\hat{x}$  more pronounced. In contrast, as it remains unclear whether the input image  $x$  is from InD or OoD, the anomaly removal on  $x$  may have a negative impact on a correct assessment of the disparity between  $x$  and  $\hat{x}$ .

**The ensemble coefficient  $\lambda$ .** In our ensemble scheme, the coefficient  $\lambda$  in Eq.(8) balances the two metrics  $\epsilon_{\text{KL}}$  and  $\epsilon_{\ell_2}$  on the representations in the probability space and feature space, respectively. A sensitivity analysis on varied values of  $\lambda$  is conducted to investigate the effect of ensembling such two metrics, with results shown in Fig.3. It can be observed from Fig.3 that a rather balanced coefficient  $\lambda = 0.5$  brings the lowest detection FPR value of  $D^3$  and thus is thereby suggested for practitioners with our  $D^3$  method. This result to some extent also indicates that the disparities based on  $\epsilon_{\text{KL}}$  and  $\epsilon_{\ell_2}$  are nearly equally important in contributing to the superior detection performances, further verifying their indispensable significance.

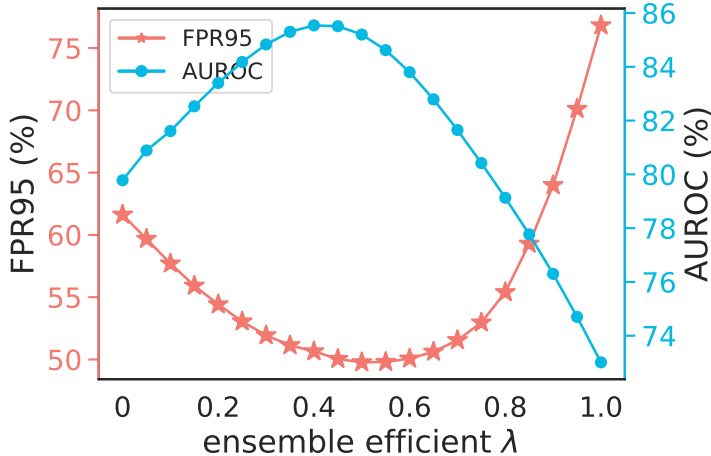


Figure 3: The average detection FPR and AUROC on multiple OoD datasets w.r.t varied coefficients  $\lambda$  of  $D^3$ .

#### 4.4 Further evaluations on diffusion models

**Conditional v.s. unconditional DMs.**  $D^3$  adopts conditional DMs to generate  $\hat{x}$  [23, 46, 38]. That is, the predictions from the classifier-under-protection are introduced in the reverse process of the DM to guide the generation of  $\hat{x}$ .

In this section, we consider the effect of using another type of DMs, i.e., unconditional DMs, where  $\hat{x}$  is recovered without any label information. The results in Tab.4 demonstrate the inferior performances of unconditional DMs than conditional DMs for  $D^3$ . The DM-generated  $\hat{x}$  with the label guidance approaches more closely towards the InD  $\mathbb{P}_{\text{in}}$  than those without the label guidance, thus contributing to a more significant distribution disparity between  $x$  and  $\hat{x}$  and improved detection performance.

Method	DMs	OoD data sets								AVERAGE	
		Species		iNaturalist		OpenImage-O		ImageNet-O		FPR↓	AUROC↑
		FPR↓	AUROC↑	FPR↓	AUROC↑	FPR↓	AUROC↑	FPR↓	AUROC↑		
$D^3$	uncond.	68.44	79.43	13.26	97.50	40.56	90.00	90.95	63.82	53.30	82.69
	cond.	<b>64.81</b>	<b>81.27</b>	<b>10.65</b>	<b>97.89</b>	<b>35.58</b>	<b>92.16</b>	<b>88.05</b>	<b>69.51</b>	<b>49.77</b>	<b>85.20</b>
$D^{3+}$	uncond.	73.38	75.75	19.41	95.89	49.13	84.00	85.50	68.51	56.86	81.04
	cond.	<b>66.45</b>	<b>81.23</b>	<b>14.67</b>	<b>97.13</b>	<b>41.93</b>	<b>88.70</b>	<b>80.25</b>	<b>75.51</b>	<b>50.82</b>	<b>85.64</b>

Table 4: Empirical results of the effects of conditional (cond.) and unconditional (uncond.) diffusion models on the detection performance of  $D^3$  and  $D^{3+}$ . The FPR and AUROC values on each OoD data set are reported.

**Effect of varied diffusion time steps.**  $D^3$  adopts the DDIM sampling [39] for fewer sampling steps  $T$  in the reverse processes of the DM. Different steps  $T$  significantly affect the quality of generated images  $\hat{x}$ , and thereby influence

the detection performance. A wide range of the diffusion timesteps  $T$  are exploited for a sensitivity analysis on the detection results of  $D^3$ , shown in Fig.4.

Generally, as the diffusion time step  $T$  increases, the quality of the generated image  $\hat{x}$  gets enhanced and approaches the InD  $\mathbb{P}_{in}$  more. Thus, the disparities between  $x$  and  $\hat{x}$  become more salient, which is beneficial for the metrics of our  $D^3$  and helps bring better detection performance under large values of the time step  $T$ , as shown in Fig.4. In the main comparisons in Tab.1, both  $D^3$  and  $D^3+$  adopt a default value of  $T = 24$  following the recommended settings in [38].

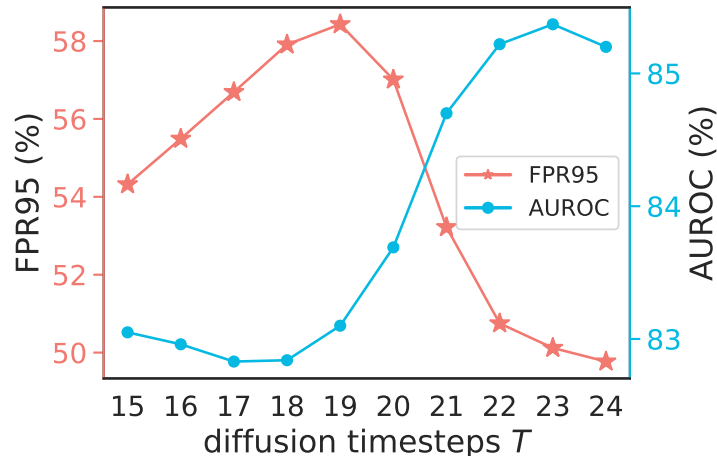


Figure 4: The average detection FPR and AUROC on multiple OoD datasets w.r.t varied diffusion time steps  $T$  of  $D^3$ .

## 5 Conclusion and discussion

In this work, we propose the  $D^3$  framework to address two main drawbacks in the image disparity assessment of existing DM-based methods: (i) the assessed objectives and (ii) the disparity metrics. For the former, the classifier-under-protection is introduced to leverage the representations in the feature and probability spaces as the assessing objectives, instead of the human-perceived image contents. For the latter, an  $\ell_2$ -distance based metric and a KL-divergence based metric are devised in the feature and probability spaces, respectively, which outperforms perceptual metrics. An anomaly-removal strategy is integrated into  $D^3$  by removing the OoD information in the DM generation to further enhance its disparity with the input image. Extensive experiments illustrate SOTA detection performance of  $D^3$  among DM-based detection methods.

The limitation of this work can lie in the computation costs in generating the synthesis  $\hat{x}$  via the DM, which is yet also a common limitation of DM-based methods. One could mitigate this issue by introducing more advanced techniques for efficient diffusion models, such as lightweight model checkpoints and faster sampling schedules.

## References

- [1] Yann LeCun, Yoshua Bengio, and Geoffrey Hinton. Deep learning. *nature*, 521(7553):436–444, 2015.
- [2] Vikash Schwag, Arjun Nitin Bhagoji, Liwei Song, Chawin Sitawarin, Daniel Cullina, Mung Chiang, and Prateek Mittal. Analyzing the robustness of open-world machine learning. In *Proceedings of the 12th ACM Workshop on Artificial Intelligence and Security*, pages 105–116, 2019.
- [3] Jingkang Yang, Kaiyang Zhou, Yixuan Li, and Ziwei Liu. Generalized out-of-distribution detection: A survey. *International Journal of Computer Vision*, pages 1–28, 2024.
- [4] Jonathan Ho, Ajay Jain, and Pieter Abbeel. Denoising diffusion probabilistic models. *Advances in neural information processing systems*, 33:6840–6851, 2020.
- [5] Mark S Graham, Walter HL Pinaya, Petru-Daniel Tudosiu, Parashkev Nachev, Sebastien Ourselin, and M Jorge Cardoso. Denoising diffusion models for out-of-distribution detection. In *2023 IEEE/CVF Conference on Computer Vision and Pattern Recognition Workshops (CVPRW)*, pages 2948–2957. IEEE, 2023.

- [6] Zhenzhen Liu, Jin Peng Zhou, Yufan Wang, and Kilian Q Weinberger. Unsupervised out-of-distribution detection with diffusion inpainting. In International Conference on Machine Learning, pages 22528–22538. PMLR, 2023.
- [7] Ruiyuan Gao, Chenchen Zhao, Lanqing Hong, and Qiang Xu. Diffguard: Semantic mismatch-guided out-of-distribution detection using pre-trained diffusion models. In Proceedings of the IEEE/CVF International Conference on Computer Vision, pages 1579–1589, 2023.
- [8] Dan Hendrycks and Kevin Gimpel. A baseline for detecting misclassified and out-of-distribution examples in neural networks. In International Conference on Learning Representations, 2016.
- [9] Weitang Liu, Xiaoyun Wang, John Owens, and Yixuan Li. Energy-based out-of-distribution detection. Advances in neural information processing systems, 33:21464–21475, 2020.
- [10] Yiyu Sun, Yifei Ming, Xiaojin Zhu, and Yixuan Li. Out-of-distribution detection with deep nearest neighbors. In International Conference on Machine Learning, pages 20827–20840. PMLR, 2022.
- [11] Kun Fang, Qinghua Tao, Kexin Lv, Mingzhen He, Xiaolin Huang, and Jie Yang. Kernel pca for out-of-distribution detection. arXiv preprint arXiv:2402.02949, 2024.
- [12] Rui Huang, Andrew Geng, and Yixuan Li. On the importance of gradients for detecting distributional shifts in the wild. Advances in Neural Information Processing Systems, 34:677–689, 2021.
- [13] Richard Zhang, Phillip Isola, Alexei A Efros, Eli Shechtman, and Oliver Wang. The unreasonable effectiveness of deep features as a perceptual metric. In Proceedings of the IEEE conference on computer vision and pattern recognition, pages 586–595, 2018.
- [14] Keyan Ding, Kede Ma, Shiqi Wang, and Eero P Simoncelli. Image quality assessment: Unifying structure and texture similarity. IEEE transactions on pattern analysis and machine intelligence, 44(5):2567–2581, 2020.
- [15] Shiyu Liang, Yixuan Li, and R Srikant. Enhancing the reliability of out-of-distribution image detection in neural networks. In International Conference on Learning Representations, 2018.
- [16] Dan Hendrycks, Steven Basart, Mantas Mazeika, Andy Zou, Joseph Kwon, Mohammadreza Mostajabi, Jacob Steinhardt, and Dawn Song. Scaling out-of-distribution detection for real-world settings. In International Conference on Machine Learning, pages 8759–8773. PMLR, 2022.
- [17] Zihan Zhang and Xiang Xiang. Decoupling maxlogit for out-of-distribution detection. In Proceedings of the IEEE/CVF Conference on Computer Vision and Pattern Recognition, pages 3388–3397, 2023.
- [18] Yingwen Wu, Tao Li, Xinwen Cheng, Jie Yang, and Xiaolin Huang. Low-dimensional gradient helps out-of-distribution detection. arXiv preprint arXiv:2310.17163, 2023.
- [19] Kimin Lee, Kibok Lee, Honglak Lee, and Jinwoo Shin. A simple unified framework for detecting out-of-distribution samples and adversarial attacks. Advances in neural information processing systems, 31, 2018.
- [20] Jaewoo Park, Yoon Gyo Jung, and Andrew Beng Jin Teoh. Nearest neighbor guidance for out-of-distribution detection. In Proceedings of the IEEE/CVF International Conference on Computer Vision, pages 1686–1695, 2023.
- [21] Yeonguk Yu, Sungho Shin, Seongju Lee, Changhyun Jun, and Kyoobin Lee. Block selection method for using feature norm in out-of-distribution detection. In Proceedings of the IEEE/CVF Conference on Computer Vision and Pattern Recognition, pages 15701–15711, 2023.
- [22] Xiaoyuan Guan, Zhouwu Liu, Wei-Shi Zheng, Yuren Zhou, and Ruixuan Wang. Revisit pca-based technique for out-of-distribution detection. In Proceedings of the IEEE/CVF International Conference on Computer Vision, pages 19431–19439, 2023.
- [23] Jascha Sohl-Dickstein, Eric Weiss, Niru Maheswaranathan, and Surya Ganguli. Deep unsupervised learning using nonequilibrium thermodynamics. In International conference on machine learning, pages 2256–2265. PMLR, 2015.
- [24] Xuefeng Du, Yiyu Sun, Jerry Zhu, and Yixuan Li. Dream the impossible: Outlier imagination with diffusion models. Advances in Neural Information Processing Systems, 36, 2024.
- [25] Junjiao Tian, Yen-Chang Hsu, Yilin Shen, Hongxia Jin, and Zsolt Kira. Exploring covariate and concept shift for out-of-distribution detection. In NeurIPS 2021 Workshop on Distribution Shifts: Connecting Methods and Applications, 2021.
- [26] Solomon Kullback and Richard A Leibler. On information and sufficiency. The annals of mathematical statistics, 22(1):79–86, 1951.
- [27] Yiyu Sun, Chuan Guo, and Yixuan Li. React: Out-of-distribution detection with rectified activations. Advances in Neural Information Processing Systems, 34:144–157, 2021.

- [28] Yao Zhu, YueFeng Chen, Chuanlong Xie, Xiaodan Li, Rong Zhang, Hui Xue, Xiang Tian, Yaowu Chen, et al. Boosting out-of-distribution detection with typical features. Advances in Neural Information Processing Systems, 35:20758–20769, 2022.
- [29] Yue Song, Nicu Sebe, and Wei Wang. Rankfeat: Rank-1 feature removal for out-of-distribution detection. Advances in Neural Information Processing Systems, 35:17885–17898, 2022.
- [30] Mingyu Xu, Zheng Lian, Bin Liu, and Jianhua Tao. Vra: Variational rectified activation for out-of-distribution detection. Advances in Neural Information Processing Systems, 36:28941–28959, 2023.
- [31] Jingkang Yang, Pengyun Wang, Dejian Zou, Zitang Zhou, Kunyuan Ding, Wenxuan Peng, Haoqi Wang, Guangyao Chen, Bo Li, Yiyu Sun, et al. Openood: Benchmarking generalized out-of-distribution detection. Advances in Neural Information Processing Systems, 35:32598–32611, 2022.
- [32] Jia Deng, Wei Dong, Richard Socher, Li-Jia Li, Kai Li, and Li Fei-Fei. Imagenet: A large-scale hierarchical image database. In IEEE Conference on Computer Vision and Pattern Recognition, pages 248–255, 2009.
- [33] A Krizhevsky. Learning multiple layers of features from tiny images. Master’s thesis, University of Toronto, 2009.
- [34] Wei He, Kai Han, Ying Nie, Chengcheng Wang, and Yunhe Wang. Species196: A one-million semi-supervised dataset for fine-grained species recognition. Advances in Neural Information Processing Systems, 36, 2024.
- [35] Grant Van Horn, Oisin Mac Aodha, Yang Song, Yin Cui, Chen Sun, Alex Shepard, Hartwig Adam, Pietro Perona, and Serge Belongie. The inaturalist species classification and detection dataset. In Proceedings of the IEEE conference on computer vision and pattern recognition, pages 8769–8778, 2018.
- [36] Haoqi Wang, Zhizhong Li, Litong Feng, and Wayne Zhang. Vim: Out-of-distribution with virtual-logit matching. In Proceedings of the IEEE/CVF Conference on Computer Vision and Pattern Recognition, pages 4921–4930, 2022.
- [37] Dan Hendrycks, Kevin Zhao, Steven Basart, Jacob Steinhardt, and Dawn Song. Natural adversarial examples. In Proceedings of the IEEE/CVF conference on computer vision and pattern recognition, pages 15262–15271, 2021.
- [38] Prafulla Dhariwal and Alexander Nichol. Diffusion models beat gans on image synthesis. Advances in neural information processing systems, 34:8780–8794, 2021.
- [39] Jiaming Song, Chenlin Meng, and Stefano Ermon. Denoising diffusion implicit models. In International Conference on Learning Representations, 2020.
- [40] Robin Rombach, Andreas Blattmann, Dominik Lorenz, Patrick Esser, and Björn Ommer. High-resolution image synthesis with latent diffusion models. In Proceedings of the IEEE/CVF conference on computer vision and pattern recognition, pages 10684–10695, 2022.
- [41] Kaiming He, Xiangyu Zhang, Shaoqing Ren, and Jian Sun. Deep residual learning for image recognition. In IEEE Conference on Computer Vision and Pattern Recognition, pages 770–778, 2016.
- [42] Gao Huang, Zhuang Liu, Laurens Van Der Maaten, and Kilian Q Weinberger. Densely connected convolutional networks. In Proceedings of the IEEE conference on computer vision and pattern recognition, pages 4700–4708, 2017.
- [43] Adam Paszke, Sam Gross, Francisco Massa, Adam Lerer, James Bradbury, Gregory Chanan, Trevor Killeen, Zeming Lin, Natalia Gimelshein, Luca Antiga, et al. Pytorch: An imperative style, high-performance deep learning library. Advances in neural information processing systems, 32, 2019.
- [44] Ziwei Liu, Ping Luo, Xiaogang Wang, and Xiaoou Tang. Deep learning face attributes in the wild. In Proceedings of the IEEE international conference on computer vision, pages 3730–3738, 2015.
- [45] Yuval Netzer, Tao Wang, Adam Coates, Alessandro Bissacco, Bo Wu, and Andrew Y Ng. Reading digits in natural images with unsupervised feature learning. In Proceedings of the NIPS Workshop on Deep Learning and Unsupervised Feature Learning, 2011.
- [46] Yang Song, Jascha Sohl-Dickstein, Diederik P Kingma, Abhishek Kumar, Stefano Ermon, and Ben Poole. Score-based generative modeling through stochastic differential equations. In International Conference on Learning Representations, 2020.

## Appendix A Supplementary empirical setups

### A.1 Details of the InD and OoD data sets

The large-scale ImageNet-1K [32] is selected as the InD data with 1,281,167 training and 50,000 test images from 1,000 categories.

The OoD data sets are outlined as below:

- Species [34] includes both labeled and unlabeled images of invasive species with bounding box annotations. For OoD detection, 10,000 images are sampled by OpenOOD [31].
- iNaturalist [35] contains natural fine-grained images of different species of plants and animals. For OoD detection, 10,000 images are sampled from the selected concepts by OpenOOD [31].
- OpenImage-O [36] is collected image-by-image from the test set of OpenImage-V3. 17,632 images are included in this data set.
- ImageNet-O [37] is gathered from the even large ImageNet-22K data set with ImageNet-1K classes deleted. The 2,000 images in ImageNet-O are even adversarial filtered, and are very hard to be distinguished from the InD ImageNet-1K data.

### A.2 Details of the baseline OoD detectors

We elaborate the details of the compared non-diffusion OoD detectors in the experiments, covering three different types of logits-, gradients-, and features-based methods.

The classifier-under-protection  $f : \mathbb{R}^d \rightarrow \mathbb{R}^C$  learns features  $\mathbf{h}_x \in \mathbb{R}^m$  before the last linear layer and outputs predictive logits  $\bar{\mathbf{g}}_x \in \mathbb{R}^C$  of the inputs  $\mathbf{x} \in \mathbb{R}^d$ . Notice that the probabilities  $\mathbf{g}_x$  in the main text are obtained by applying a softmax function on the logits  $\bar{\mathbf{g}}_x$ .

**MSP** [8] takes the maximum value of probabilities of  $\mathbf{x}$  from the classifier-under-protection as the scoring function:

$$S_{\text{MSP}}(\mathbf{x}) = \max(\text{softmax}(\bar{\mathbf{g}}_x)) = \max(\mathbf{g}_x). \quad (9)$$

**ODIN** [15] improves MSP by applying the temperature scaling on the logits of the adversarial examples of  $\mathbf{x}$ :

$$S_{\text{ODIN}}(\mathbf{x}) = \max(\text{softmax}(\frac{\bar{\mathbf{g}}_{adv}}{T})). \quad (10)$$

$\mathbf{x}_{adv}$  denotes the adversarial examples of  $\mathbf{x}$ , and  $T$  indicates the temperature coefficient.

**Energy** [9] applies the energy function on the logits  $\bar{\mathbf{g}}_x$  of the inputs  $\mathbf{x}$  from the classifier-under-protection. The analysis [44] shows that energy is well aligned with the input probability density.

$$S_{\text{Energy}}(\mathbf{x}) = \log \sum_{i=1}^C \exp(\bar{\mathbf{g}}_x[i]), \quad (11)$$

where  $\bar{\mathbf{g}}_x[i]$  indicates the  $i$ -th element in the  $C$ -dimensional logits  $\bar{\mathbf{g}}_x \in \mathbb{R}^C$ .

**GradNorm** [12] proposes a novel loss as the KL divergence between the probabilities of  $\mathbf{x}$  and a uniform distribution  $\mathbf{u} = [1/C, \dots, 1/C] \in \mathbb{R}^C$ , and then take the gradients w.r.t this loss on the weight parameter  $\mathbf{W} \in \mathbb{R}^{m \times C}$  of the last linear layer in the classifier-under-protection. The  $\ell_1$  norm of the gradients is verified as an effective detection score:

$$S_{\text{GradNorm}}(\mathbf{x}) = \left\| \frac{\partial \text{KL}(\mathbf{g}_x \parallel \mathbf{u})}{\partial \mathbf{W}} \right\|_1. \quad (12)$$

**ViM** [36] combines the logits and features together from the classifier-under-protection for OoD detection. Firstly, all the training features are gathered and the residual subspace is extracted by PCA. Then, in the inference stage, the features  $\mathbf{h}_x$  of a new sample  $\mathbf{x}$  is projected to the residual space, and the norm of the projected feature is computed. After that, the projected feature norm is put as an additional dimension in the logits  $\bar{\mathbf{g}}_x$ , and the extended logits get normalized via the softmax function. Finally, the value of the normalized projected feature norm is set as the detection score.

**KNN** [10] is a simple and effective OoD detection method also with significantly heavy memory and time costs, as all the  $N_{\text{tr}}$  training features have to be stored and iterated. The nearest neighbor searching is executed between the features

of the new sample and all the features of the training data. The negative of the ( $k$ -th) shortest  $\ell_2$  distance is set as the detection score:

$$S_{\text{KNN}}(\mathbf{x}) = - \min_{i:1,\dots,N_{\text{tr}}} \left\| \frac{\mathbf{h}_{\mathbf{x}}}{\|\mathbf{h}_{\mathbf{x}}\|_2} - \frac{\mathbf{h}_{\mathbf{x}_{\text{tr}}}^i}{\|\mathbf{h}_{\mathbf{x}_{\text{tr}}}^i\|_2} \right\|_2, \quad (13)$$

where  $\mathbf{h}_{\mathbf{x}_{\text{tr}}}^i$  denotes penultimate features of the  $i$ -th training sample.

MLS [16] claims that the classic MSP does not well scale to large-scale challenging data sets, and instead proposes that the maximum logits are superior in large-scale and multi-class anomaly segmentation:

$$S_{\text{MLS}}(\mathbf{x}) = \max(\bar{\mathbf{g}}_{\mathbf{x}}). \quad (14)$$

### A.3 Implementation details

**Image pre-processing.** In the forward and reverse diffusion processes of the DMs, the test images are resized and cropped to  $256 \times 256 \times 3$  and normalized to  $[-1, 1]$ , following the requirements of the released checkpoints of diffusion models in [38]. Then, in the forward procedure of the classifier-under-protection, those test images and their generated counterparts are resized to  $224 \times 224 \times 3$  with the mean-variance normalization, as required by the PyTorch-released checkpoints of the classifier-under-protection.

**Hyper-parameters.** In the part of image synthesis via diffusion models,  $D^3$  and  $D^{3+}$  adopt the recommended settings in [38], see detailed hyper-parameters of diffusion models in both the released code of [38] and ours.

In the part of the boosting strategy of  $D^3$  and  $D^{3+}$ , for the ReAct in  $D^3$ , the threshold  $c$  in Eq.(7) is specified as  $c = 0.1$  to acquire the features  $\mathbf{h}_{\hat{\mathbf{x}}}^{\text{ReAct}}$  and logits  $\mathbf{g}_{\hat{\mathbf{x}}}^{\text{ReAct}}$  for both ResNet50 and DenseNet121. For the VRA in  $D^{3+}$ , the features  $\mathbf{h}_{\hat{\mathbf{x}}}^{\text{VRA}}$  are kept the same as  $\mathbf{h}_{\hat{\mathbf{x}}}^{\text{ReAct}}$ , and the thresholds  $\alpha, \beta$  in Eq.(7) are specified as  $\alpha = 0.1, \beta = 0.5$  to obtain the logits  $\mathbf{g}_{\hat{\mathbf{x}}}^{\text{VRA}}$  for ResNet50 and  $\alpha = 0.1, \beta = 0.2$  for DenseNet121.

In the part of the ensemble of  $D^3$  and  $D^{3+}$  in Eq.(8), the disparities  $\epsilon_{\text{KL}}, \epsilon_{\ell_2}$  from probabilities and features belong to different orders of magnitude. Therefore,  $\epsilon_{\text{KL}}$  and  $\epsilon_{\ell_2}$  are supposed to be normalized before the ensemble. To be specific, we adopt the min-max normalization on  $\epsilon_{\text{KL}}$  and  $\epsilon_{\ell_2}$  with the maximum and minimum values of the available InD data, respectively. In addition, the coefficient  $\lambda$  in ensemble is specified as  $\lambda = 0.5$  for  $D^3$ ,  $\lambda = 0.45$  for  $D^{3+}$  of ResNet50 and  $\lambda = 0.65$  for  $D^{3+}$  of DenseNet121.

Regarding the GPU resources, experiments for the image synthesis via diffusion models are executed parallelly on 4 NVIDIA v100 GPUs, and experiments for the forward procedure in the classifier-under-protection are executed on 1 NVIDIA GeForce RTX 3090 GPU.

## Appendix B Supplementary empirical results

Table 5 illustrates the comparison detection results with the classifier-under-protection of DenseNet121 trained on ImageNet-1K as the InD data. Our  $D^3$  and  $D^{3+}$  keep superior detection performance on DenseNet121 over other non-diffusion-based and diffusion-based OoD detectors with lowest FPR and high AUROC values averaged on the OoD data sets. The DDPM detector [5] does not rely on the classifier-under-protection and thus shows the same detection performance as that of ResNet50. We are unable to reproduce DiffGuard [7] on DenseNet121 based on the released code and have to omit the comparison here. Table 5 and Table 1 in the main text together validate the effectiveness of our distribution disparity metric in diffusion-based detection.

method	OoD data sets								AVERAGE	
	Species		iNaturalist		OpenImage-O		ImageNet-O			
	FPR↓	AUROC↑	FPR↓	AUROC↑	FPR↓	AUROC↑	FPR↓	AUROC↑	FPR↓	AUROC↑
<i>non-diffusion-based</i>										
MSP [8]	80.29	<u>74.75</u>	49.28	89.05	66.80	83.83	98.65	47.39	73.76	73.76
ODIN [15]	79.59	<u>72.56</u>	39.57	92.81	57.65	88.49	97.50	56.41	68.58	77.57
Energy [9]	80.25	71.66	39.70	92.66	56.51	88.49	96.45	57.46	68.23	77.57
GradNorm [12]	79.35	69.36	26.70	93.40	55.27	80.66	92.35	54.68	63.42	74.53
ReAct [27]	77.64	77.65	46.87	90.30	67.97	73.93	93.00	48.35	71.37	72.56
KNN [10]	85.77	73.58	86.52	74.91	67.26	81.03	<b>69.85</b>	<b>81.64</b>	77.35	77.79
MLS [16]	79.59	<u>72.56</u>	39.58	92.81	57.63	88.49	97.50	56.40	68.58	77.57
VRA [30]	76.00	75.05	33.71	93.05	55.29	82.49	85.00	63.74	62.50	78.58
<i>diffusion-based</i>										
DDPM [5]	96.86	44.97	96.27	48.70	94.41	49.35	91.55	51.73	94.77	48.69
D <sup>3</sup>	<u>75.55</u>	<b>75.08</b>	<u>20.13</u>	<u>96.19</u>	<u>44.95</u>	<u>88.82</u>	<u>74.55</u>	<u>79.20</u>	<u>53.79</u>	<b>84.82</b>
D <sup>3+</sup>	<b>75.42</b>	72.10	<b>19.07</b>	<b>96.37</b>	<b>40.68</b>	<b>90.98</b>	77.95	76.53	<b>53.28</b>	<u>83.99</u>

Table 5: The detection performance of various OoD detectors (**DenseNet121** on **ImageNet-1K**). The **best** and runner-up results are highlighted with bold fonts and underlines, respectively.